International Journal of Solids and Structures 51 (2014) 1954–1961

Contents lists available at ScienceDirect

International Journal of Solids and Structures

journal homepage: www.elsevier.com/locate/ijsolstr

Elastic fields due to dislocation arrays in anisotropic bimaterials

Haijian Chu [a,*], Ernian Pan [b]

[a] Department of Mechanics, Shanghai University, Shanghai 200444, China
[b] Computer Modeling and Simulation Group, University of Akron, Akron, OH 44325, USA

ARTICLE INFO

Article history:
Received 5 March 2013
Received in revised form 21 December 2013
Available online 18 February 2014

Keywords:
Dislocations arrays
Anisotropic bimaterial
Green's function
Stroh formalism
Peach–Koehler force

ABSTRACT

Based on the single-dislocation Green's function, analytical solutions of the elastic fields due to dislocation arrays in an anisotropic bimaterial system are derived by virtue of the Cottrell summation formula. The singularity in the Peach–Koehler (P–K) force is removed by both rigorous mathematical approach and physical energy consideration. Numerical results for dislocation arrays in the Cu/Nb bimaterial with Kurdjumov–Sachs (K–S) orientation show that: (1) the traction continuity and periodic condition are both satisfied; (2) the maximum magnitude of the traction at the interface due to a mixed dislocation array is smaller than that due to a single mixed dislocation. In other words, the traction at the interface could be suppressed by the corresponding array with a relatively high density ($L < 10$ nm); however, the shear stress on the glide plane increases with increasing dislocation density; (3) the Cu/Nb interface attracts the mixed dislocation array in copper and repels the screw one there. This implies that the P–K force depends not only on the material properties, but also on the crystal orientation and the type of Burgers vector, among others.

1. Introduction

The line defect of dislocations, by offering a highly effective approach to produce plastic deformation, controls many important macroscale properties of a material, such as the material strength, electric conductivity and optical properties (Zhu and Li, 2010; Otsuka et al., 2003; Ohno et al., 2012; Pennycook, 2008; Chen et al., 2008). Within a crystal, dislocations could nucleate from the sessile sites (e.g. Frank–Read source), grain boundaries or interfaces between two different phases (Beausir and Fressengeas, 2013). The dynamic activity of a dislocation, such as gliding, cross-slip, annihilation, pileup, and tangles, plays a critical role in the behavior of the material (Ghoniem and Han, 2005; Wang and Beyerlein, 2011; Zhou et al., 2010). In specific circumstances, dislocations could concentrate themselves in a certain region to reduce the total energy so that other regions would be free of dislocations. Thus, dislocation array or dislocation wall, such as tilt wall with edge dislocations, twist wall with screw dislocations, would be formed. The dislocation array can also form during the fabrication of multilayer materials due to the lattice mismatch between the substrate and the deposited layer (Krasavin, 2009) (sometimes between the buffer layer and the deposited layer). HRTEM images of silver shows three sets of dislocation walls with Shockley partials aligning at the incoherent twin boundary; among them, one set acts as the front tip of the deformation twins and deviates from the boundary a few nanometers (Liu et al., 2011). Such phenomena were also predicted recently via molecular simulation. In terms of its stability, there are three different sets of dislocation array in Kurdjumov–Sachs (K–S) {112} interface in Cu/Nb (fcc/bcc) bimaterial (Kang et al., 2012): two sets are located at the interface, and one set deviates from the interface. Similar results were also observed in Cu/Fe (fcc/bcc) bimaterial. In molecular simulations, periodic boundary conditions (PBCs) (Subramaniyan and Sun, 2008) are often assumed due to the limitation of the modeling size. In order to study the dislocation effect, one may insert/build a dislocation in the model. As a consequence of PBC, the model inherently includes a series of dislocations or dislocation array. The challenging issue is how to set the original positions of the atoms and their boundaries in the molecular model. As such, the elastic field due to the dislocation array is needed in building the dislocation-array model in molecular simulation. It should be noted that, due to the nonlinear elastic property in dislocation core region, the linear elastic solution cannot be used to the core region.

To understand the dislocations motion, extensive work has been carried out on the elastic fields due to the dislocation (e.g. Lubarda, 1997; Cai et al., 2001; Gutkin et al., 2013). The fundamental solutions due to an individual dislocation in isotropic/anisotropic infinite media and bimaterial were derived. For instance, based on the Green's function method, Mura (1963, 1987) proposed a line-integral expression for the stress field due to a dislocation in an isotropic elastic and infinite medium where the symmetry

* Corresponding author. Tel.: +86 2166136103.
E-mail address: hjchu01@gmail.com (H. Chu).

http://dx.doi.org/10.1016/j.ijsolstr.2014.02.001
0020-7683/

property of the corresponding Green's function was applied. Gosling and Willis (1994a) developed a line-integral representation for the stress field due to an arbitrary dislocation loop in an isotropic half space. Based on the Stroh formalism and Fourier transform, Chu et al. (2011a, 2012a,b) recently presented a line-integral expression for the elastic field due to a polygonal-shape dislocation loop in anisotropic full, half, and bimaterial spaces where the Green's functions obtained by Pan and Yuan (2000) were used. Using the Galerkin potential function and Fourier transform, Tan and Sun (2006, 2011) derived the point-force Green's function for a multilayered heterogeneous thin film and proposed a line-integral expression for the dislocation-induced stress field.

The elastic fields due to a dislocation array or wall can be obtained by superposing the contributions of all the dislocations in the wall (e.g. Chou, 1962; Hartley, 1969; Nakahara et al., 1972; Chou and Lin, 1975; Rey and Saada, 1975; Hirth et al., 1979; Lubarda and Kouris, 1996). Chou (1962) obtained the stress field due to an equally spaced straight dislocation array in the basal planes in a hexagonal crystal. Hirth et al. (1979) derived the stress field of a dislocation array located at the interface of bicrystals and solved the long-range field issue. The Cottrell summation formula (Cottrell, 1953) was used by Hirth and Lothe (1982) for dealing with the dislocation array in isotropic material, and simple expressions for the stress field were obtained. Gosling and Willis (1994b) calculated the energy of a dislocation array in an anisotropic half space. Lubarda (1997) obtained the elastic energy due to a dislocation array which are near the bimaterial interface or near the free surface of an isotropic half space. Recently, de Geus et al. (2014) studied the stress field due to dislocation walls with pile-up in a homogeneous isotropic full space. However, the influence of anisotropy in bicrystals is seldom explored.

In this paper, we derive the elastic field due to a dislocation array in an anisotropic and elastic bimaterial system. Based on the exact closed-form solutions of the induced strain and stress fields, we then investigate the influence of the interface and the period length of the dislocation array on the elastic field and P–K force. This paper is organized as follows. The Green's function due to a single dislocation in an anisotropic bimaterial system is briefly reviewed in Section 2. The elastic field due to the dislocation array is derived and the P–K force is investigated in Section 3. For the important Cu/Nb bimaterial system, the influence of the interface and period length of the dislocation array on the stress field and P–K force is illustrated numerically in Section 4. Finally, conclusions are drawn in Section 5.

2. Green's functions due to a dislocation in bimaterial

The elastic fields due to a single dislocation in isotropic or anisotropic bimaterial were studied in previous literature (Dundurs and Mura, 1964; Barnett and Lothe, 1974; Ting, 1996). For completeness of the topic studied here, we present only the main results in terms of the Stroh formalism (Stroh, 1958, 1962) as follows.

We assume that Materials 1 and 2 occupy the half plane z > 0 and z < 0, respectively, and that the dislocation with Burgers vector $\boldsymbol{b} = (\Delta u_1, \Delta u_2, \Delta u_3)$ is located at (X,Z) in the half plane of Material λ (λ = 1 or 2). Then if the field point $\boldsymbol{x} = (x,z)$ is in Material λ, the displacement and traction vectors can be expressed as (Ting, 1996):

$$\begin{aligned}\boldsymbol{u}^\lambda &= \frac{1}{\pi}\mathrm{Im}\left\{\boldsymbol{A}^\lambda\langle\ln(z_*^\lambda - s_*^\lambda)\rangle\boldsymbol{q}^{\infty,\lambda}\right\} + \frac{1}{\pi}\mathrm{Im}\sum_{j=1}^{3}\left\{\boldsymbol{A}^\lambda\left\langle\ln\left(z_*^\lambda - \bar{s}_j^\lambda\right)\right\rangle\boldsymbol{q}_j^\lambda\right\}\\ \boldsymbol{t}^\lambda &= -\frac{1}{\pi}\mathrm{Im}\left\{\boldsymbol{B}^\lambda\left\langle\frac{p_*^\lambda n_1 - n_3}{z_*^\lambda - s_*^\lambda}\right\rangle\boldsymbol{q}^{\infty,\lambda}\right\} - \frac{1}{\pi}\mathrm{Im}\sum_{j=1}^{3}\left\{\boldsymbol{B}^\lambda\left\langle\frac{p_*^\lambda n_1 - n_3}{z_*^\lambda - \bar{s}_j^\lambda}\right\rangle\boldsymbol{q}_j^\lambda\right\}\end{aligned} \tag{1}$$

If the field point (x,z) is in the other half-plane, i.e., Material μ ($\mu \neq \lambda$) (λ, μ = 1 or 2), then the displacement and traction vectors can be expressed as:

$$\begin{aligned}\boldsymbol{u}^\mu &= \frac{1}{\pi}\mathrm{Im}\sum_{j=1}^{3}\left\{\boldsymbol{A}^\mu\left\langle\ln\left(z_*^\mu - s_j^\lambda\right)\right\rangle\boldsymbol{q}_j^\mu\right\}\\ \boldsymbol{t}^\mu &= -\frac{1}{\pi}\mathrm{Im}\sum_{j=1}^{3}\left\{\boldsymbol{B}^\mu\left\langle\frac{p_*^\mu n_1 - n_3}{z_*^\mu - s_j^\lambda}\right\rangle\boldsymbol{q}_j^\mu\right\}\end{aligned} \tag{2}$$

In Eqs. (1) and (2), an overbar means complex conjugate; the superscripts λ and μ denote, respectively, the quantity associated with Materials λ and μ; p_j^λ, $\boldsymbol{A}^\lambda$, and $\boldsymbol{B}^\lambda$ are the Stroh eigenvalues and the corresponding eigenmatrices. Also in Eqs. (1) and (2),

$$\begin{aligned}\langle\ln(z_*^\lambda - s_*^\lambda)\rangle &= diag[\ln(z_1^\lambda - s_1^\lambda), \ln(z_2^\lambda - s_2^\lambda), \ln(z_3^\lambda - s_3^\lambda)]\\ \left\langle\ln\left(z_*^\lambda - \bar{s}_j^\lambda\right)\right\rangle &= diag\left[\ln\left(z_1^\lambda - \bar{s}_j^\lambda\right), \ln\left(z_2^\lambda - \bar{s}_j^\lambda\right), \ln\left(z_3^\lambda - \bar{s}_j^\lambda\right)\right]\end{aligned} \tag{3}$$

and

$$\begin{aligned}\left\langle\frac{1}{z_*^\lambda - s_*^\lambda}\right\rangle &= diag\left[\frac{1}{z_1^\lambda - s_1^\lambda}, \frac{1}{z_2^\lambda - s_2^\lambda}, \frac{1}{z_3^\lambda - s_3^\lambda}\right]\\ \left\langle\frac{1}{z_*^\lambda - \bar{s}_j^\lambda}\right\rangle &= diag\left[\frac{1}{z_1^\lambda - \bar{s}_j^\lambda}, \frac{1}{z_2^\lambda - \bar{s}_j^\lambda}, \frac{1}{z_3^\lambda - \bar{s}_j^\lambda}\right]\end{aligned} \tag{4}$$

where z_j^α and s_j^α ($\alpha = 1,2$) are complex variables associated with the field and source points, respectively. They are defined as:

$$z_j^\alpha = x + p_j^\alpha z, \quad s_j^\alpha = X + p_j^\alpha Z \tag{5}$$

We point out that the first term in Eq. (1) corresponds to the full-plane dislocation Green's functions in Material λ with

$$\boldsymbol{q}^{\infty,\lambda} = (\boldsymbol{B}^\lambda)^T\boldsymbol{b} \tag{6}$$

whilst the second term in Eq. (1), called also the image part, is the complementary part of the dislocation Green's function solutions due to the interface or the inhomogeneity of the two half-planes. The complex vectors $\boldsymbol{q}_j^{(\lambda)}$ (λ = 1,2; j = 1,2,3) in Eq. (1) and $\boldsymbol{q}_j^{(\mu)}$ (μ = 1,2; j = 1,2,3) in Eq. (2) are determined using the continuity conditions along the interface of the two half-planes. For a perfect interface and after some algebraic calculations, these unknown vectors can be obtained as (λ, μ = 1 or 2, but $\mu \neq \lambda$):

$$\begin{aligned}\boldsymbol{q}_j^\lambda &= (\boldsymbol{A}^\lambda)^{-1}(\boldsymbol{M}^\lambda + \overline{\boldsymbol{M}}^\mu)^{-1}(\overline{\boldsymbol{M}}^\mu - \overline{\boldsymbol{M}}^\lambda)\overline{\boldsymbol{A}}^\lambda\boldsymbol{I}_j\overline{\boldsymbol{q}}^{\infty,\lambda}\\ \boldsymbol{q}_j^\mu &= (\boldsymbol{A}^\mu)^{-1}(\overline{\boldsymbol{M}}^\lambda + \boldsymbol{M}^\mu)^{-1}(\boldsymbol{M}^\lambda + \overline{\boldsymbol{M}}^\lambda)\boldsymbol{A}^\lambda\boldsymbol{I}_j\boldsymbol{q}^{\infty,\lambda}\end{aligned} \tag{7}$$

with

$$\begin{aligned}&\boldsymbol{M}^\alpha = -i\boldsymbol{B}^\alpha(\boldsymbol{A}^\alpha)^{-1} \quad (\alpha = 1,2)\\ &\boldsymbol{I}_1 = diag[1,0,0]; \quad \boldsymbol{I}_2 = diag[0,1,0]; \quad \boldsymbol{I}_3 = diag[0,0,1]\end{aligned} \tag{8}$$

Similar Green's function expressions can be derived for a half plane or bimaterial with general (or imperfect) surface/interface conditions. Detailed discussion can be found in the references (Pan, 2003a,b). We point out that linear elasticity is assumed in deriving these solutions, and thus the solutions are not suitable for the dislocation core region where nonlinearity exists.

3. Elastic fields due to a dislocation array parallel to the interface

We now consider an infinite dislocation array parallel to the bicrystal interface as shown in Fig. 1. The space between two adjacent dislocations is L, which is also called period length of the dislocation array. We take the derivative of displacements in Eqs. (1) and (2) with respect to field point $\boldsymbol{x}$, which gives us

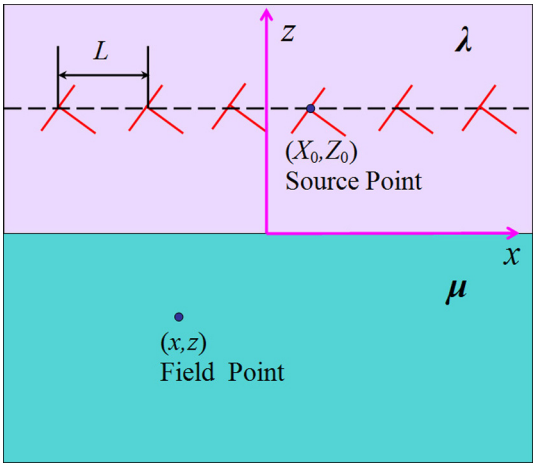

Fig. 1. Illustration of a dislocation array in a bicrystal system denoted by λ and μ. The period length of the array is L, (X_0,Z_0) represents the single dislocation source point or one of the dislocation sources in an array, and (x,z) is the field point. For the system Cu/Nb used in the numerical example, Cu is in the upper half plane, Nb in the lower half plane. The coordinate x is parallel to $[11-2]_{Cu}$ and $[1-12]_{Nb}$, z to $[111]_{Cu}$ and $[110]_{Nb}$, and y points into the plane of the paper and parallel to $[-110]_{Cu}$ and $[1-1-1]_{Nb}$.

$$\boldsymbol{u}^{\lambda}_{,i} = \frac{1}{\pi}\mathrm{Im}\left\{\boldsymbol{A}^{\lambda}\left\langle\frac{1}{z^{\lambda}_{*}-s^{\lambda}_{*}}\frac{\partial z^{\lambda}_{*}}{\partial x_i}\right\rangle\boldsymbol{q}^{\infty,\lambda}\right\} + \frac{1}{\pi}\mathrm{Im}\sum_{j=1}^{3}\left\{\boldsymbol{A}^{\lambda}\left\langle\frac{1}{z^{\lambda}_{*}-\bar{s}^{\lambda}_{j}}\frac{\partial z^{\lambda}_{*}}{\partial x_i}\right\rangle\boldsymbol{q}^{\lambda}_{j}\right\}$$
$$\boldsymbol{u}^{\mu}_{,i} = \frac{1}{\pi}\mathrm{Im}\sum_{j=1}^{3}\left\{\boldsymbol{A}^{\mu}\left\langle\frac{1}{z^{\mu}_{*}-s^{\lambda}_{j}}\frac{\partial z^{\mu}_{*}}{\partial x_i}\right\rangle\boldsymbol{q}^{\mu}_{j}\right\} \tag{9}$$

Then the derivative of displacements due to the dislocation array can be found by summing Eq. (9) over all the dislocations. Namely

$$\begin{aligned}\boldsymbol{u}^{\lambda}_{,i} &= \frac{1}{\pi}\mathrm{Im}\left\{\boldsymbol{A}^{\lambda}\left\langle\sum_{n=-\infty}^{\infty}\frac{1}{z^{\lambda}_{*}-s^{\lambda}_{*}(n)}\frac{\partial z^{\lambda}_{*}}{\partial x_i}\right\rangle\boldsymbol{q}^{\infty,\lambda}\right\} \\ &\quad + \frac{1}{\pi}\mathrm{Im}\sum_{j=1}^{3}\left\{\boldsymbol{A}^{\lambda}\left\langle\sum_{n=-\infty}^{\infty}\frac{1}{z^{\lambda}_{*}-\bar{s}^{\lambda}_{j}(n)}\frac{\partial z^{\lambda}_{*}}{\partial x_i}\right\rangle\boldsymbol{q}^{\lambda}_{j}\right\}\boldsymbol{u}^{\mu}_{,i} \\ &= \frac{1}{\pi}\mathrm{Im}\sum_{j=1}^{3}\left\{\boldsymbol{A}^{\mu}\left\langle\sum_{n=-\infty}^{\infty}\frac{1}{z^{\mu}_{*}-s^{\lambda}_{j}(n)}\frac{\partial z^{\mu}_{*}}{\partial x_i}\right\rangle\boldsymbol{q}^{\mu}_{j}\right\}\end{aligned} \tag{10}$$

where

$$s^{\lambda}_{*}(n) \equiv (X_0 - nL) + p^{\lambda}_{*}Z_0 \tag{11}$$

According to Eq. (5), we have

$$\frac{\partial z^{\alpha}_{*}}{\partial x_i} = \delta_{i1} + p^{\alpha}_{*}\delta_{i3} \quad (\alpha = \lambda \text{ or } \mu) \tag{12}$$

Thence, the summation term in Eq. (10) can be finally simplified to the similar expressions below

$$\begin{aligned}\sum_{n=-\infty}^{\infty}\frac{1}{z^{\lambda}_{*}-s^{\lambda}_{*}(n)}\frac{\partial z^{\lambda}_{*}}{\partial x_i} &= \sum_{n=-\infty}^{\infty}\frac{\delta_{i1}+p^{\lambda}_{*}\delta_{i3}}{nL+z^{\lambda}_{*}-s^{\lambda}_{*}(0)} \\ \sum_{n=-\infty}^{\infty}\frac{1}{z^{\lambda}_{*}-\bar{s}^{\lambda}_{j}(n)}\frac{\partial z^{\lambda}_{*}}{\partial x_i} &= \sum_{n=-\infty}^{\infty}\frac{\delta_{i1}+p^{\lambda}_{*}\delta_{i3}}{nL+z^{\lambda}_{*}-\bar{s}^{\lambda}_{j}(0)} \\ \sum_{n=-\infty}^{\infty}\frac{1}{z^{\mu}_{*}-s^{\lambda}_{j}(n)}\frac{\partial z^{\mu}_{*}}{\partial x_i} &= \sum_{n=-\infty}^{\infty}\frac{\delta_{i1}+p^{\mu}_{*}\delta_{i3}}{nL+z^{\mu}_{*}-s^{\lambda}_{j}(0)}\end{aligned} \tag{13}$$

This type of summation can be represented by an elementary function via the following Cottrell formula (Cottrell, 1953; Hirth and Lothe, 1982),

$$\pi\cot\pi z = \sum_{-\infty}^{\infty}\frac{1}{n+z} \tag{14}$$

Therefore, Eq. (10) becomes

$$\begin{aligned}\boldsymbol{u}^{\lambda}_{,i} &= \frac{1}{L}\mathrm{Im}\left\{\boldsymbol{A}^{\lambda}\left\langle\cot\left(\pi\frac{z^{\lambda}_{*}-s^{\lambda}_{*}(0)}{L}\right)(\delta_{i1}+p^{\lambda}_{*}\delta_{i3})\right\rangle\boldsymbol{q}^{\infty,\lambda}\right\} \\ &\quad + \frac{1}{L}\mathrm{Im}\sum_{j=1}^{3}\left\{\boldsymbol{A}^{\lambda}\left\langle\cot\left(\pi\frac{z^{\lambda}_{*}-\bar{s}^{\lambda}_{j}(0)}{L}\right)(\delta_{i1}+p^{\lambda}_{*}\delta_{i3})\right\rangle\boldsymbol{q}^{\lambda}_{j}\right\} \\ \boldsymbol{u}^{\mu}_{,i} &= \frac{1}{L}\mathrm{Im}\sum_{j=1}^{3}\left\{\boldsymbol{A}^{\mu}\left\langle\cot\left(\pi\frac{z^{\mu}_{*}-s^{\lambda}_{j}(0)}{L}\right)(\delta_{i1}+p^{\mu}_{*}\delta_{i3})\right\rangle\boldsymbol{q}^{\mu}_{j}\right\}\end{aligned} \tag{15}$$

In index notation, Eq. (15) becomes

$$\begin{aligned}u^{\lambda}_{i,j} &= \frac{1}{L}\mathrm{Im}\left\{A^{\lambda}_{ik}q^{\infty,\lambda}_{k}\cot\left(\pi\frac{z^{\lambda}_{k}-s^{\lambda}_{k}(0)}{L}\right)(\delta_{j1}+p^{\lambda}_{k}\delta_{j3})\right\} \\ &\quad + \frac{1}{L}\mathrm{Im}\sum_{l=1}^{3}\left\{A^{\lambda}_{ik}q^{\lambda}_{lk}\cot\left(\pi\frac{z^{\lambda}_{k}-\bar{s}^{\lambda}_{l}(0)}{L}\right)(\delta_{j1}+p^{\lambda}_{k}\delta_{j3})\right\} \\ u^{\mu}_{i,j} &= \frac{1}{L}\mathrm{Im}\sum_{l=1}^{3}\left\{A^{\mu}_{ik}q^{\mu}_{lk}\cot\left(\pi\frac{z^{\mu}_{k}-s^{\lambda}_{j}(0)}{L}\right)(\delta_{j1}+p^{\mu}_{k}\delta_{j3})\right\}\end{aligned} \tag{16}$$

Eqs. (15) and (16) are the main results of this paper. It is clear that the strain and its corresponding stress can be separated into two parts, one corresponding to the infinite plane and the other called image part due to the effect of the interface. This formulation is similar to the result due to a single dislocation.

With Eq. (15) or (16), we can easily find the strain field and thus the stress field in both materials. For instance, the stress field in Material λ is

$$\sigma^{\lambda}_{ij} = C^{\lambda}_{ijkl}u^{\lambda}_{k,l} \tag{17}$$

Again, Eqs. (15)–(17) apply only to the outside region of dislocation cores.

The P–K force of a dislocation is very important in the simulation of dislocation dynamics (Ghoniem and Han, 2005; Wang and Beyerlein, 2011; Zhou et al., 2010). Without lose of generality, let us consider the P–K force on the dislocation source point (X_0,Z_0) as shown in Fig. 1. The formula of the P–K force is

$$\mathbf{F} = [\mathbf{b}\cdot\boldsymbol{\sigma}(X_0,Z_0)]\times\xi \tag{18}$$

where $\mathbf{b}$ is the Burgers vector, $\boldsymbol{\sigma}(X_0,Z_0)$ is the stress tensor at the dislocation source point, and ξ is the sense of the dislocation line (Hirth and Lothe, 1982). After carefully checking the stress, one may find a major challenge in computing the P–K force using Eq. (18) directly because of the well-known singularity inside the core region. Thus, we cannot use Eq. (17) combining with Eq. (15), (16) directly. However, by examining Eq. (10), one can easily detect that the singularity is actually induced by the dislocation source at (X_0, Z_0); all other sources will not induce any singularity when considering the P–K force at (X_0, Z_0). Furthermore, without remotely applied stress, the P–K force for a straight dislocation in an infinite homogeneous medium is zero due to dislocation self-equilibrium (Eshelby, 1951). In other words, the P–K force at (X_0,Z_0) due to the singularity stress induced by the straight dislocation at (X_0,Z_0) is zero! Therefore, the singularity term in Eq. (10) can be simply abandoned when calculating the P–K force. Since we have to abandon the singularity term in Eq. (10), we cannot use Cottrell formula in Eq. (14) to find Eqs. (15) or (16) (due to the lack of the term with $n = 0$). However, we can directly sum the terms one by one as briefly presented below.

When the field point is coincident with the source point (X_0, Z_0), we have,

$$z^{\lambda}_{*} - s^{\lambda}_{*}(n)\big|_{(X_0,Z_0)} = X_0 + p^{\lambda}_{*}Z_0 - (X_0 - nL) - p^{\lambda}_{*}Z_0 = nL \tag{19}$$

where Eqs. (5) and (11) are used.

After abandoning the singularity term and making use of Eq. (19), the first summation term in $\boldsymbol{u}^{\lambda}_{,i}$ becomes

$$\frac{1}{\pi}\mathrm{Im}\left\{\boldsymbol{A}^{\lambda}\left\langle\sum_{n=-\infty}^{-1}\frac{1}{nL}\frac{\partial z_*^{\lambda}}{\partial x_i}+\sum_{n=1}^{\infty}\frac{1}{nL}\frac{\partial z_*^{\lambda}}{\partial x_i}\right\rangle\Bigg|_{(X_0,Z_0)}\boldsymbol{q}^{\infty,\lambda}\right\}=0 \tag{20}$$

Thence, the first summation term in the first expression in Eq. (15) or (16) can be simply neglected when calculating the P–K force on the dislocation source. In other words, only the image stress has contributions to the P–K force. The physical reason on neglecting the summation term in Eq. (20) can be simply explained as follows: If one considers the same dislocation array but located in two different places in an infinite homogenous crystal, it is obvious that the configurations of the two cases will be exactly the same. Thus there is no energy difference between the two configurations. Consequently, the P–K force is zero.

4. Applications to Cu/Nb (fcc/bcc) bimaterials

In this section, the well-known fcc/bcc interface with K-S orientation is taken as an example to show the influence of the dislocation array density in Cu/Nb binary on the stress field and P–K force. This low energy interface is often observed in epitaxial growth (Misra et al., 1998). Referring to Fig. 1, we assign the upper half plane to be copper Cu where the dislocations are located, and the lower half plane niobium Nb. The x-axis is parallel to $[11\text{–}2]_{Cu}$ and $[1\text{–}12]_{Nb}$, the z-axis parallel to $[111]_{Cu}$ and $[110]_{Nb}$, and the y-axis pointing into the paper is parallel to $[-110]_{Cu}$ and $[1-1-1]_{Nb}$. The mixed dislocation array has a Burgers vector ½[101] within the glide plane (11–1). Both Cu and Nb are cubic crystal and their elastic moduli are (in GPa): C_{11} = 168.4, C_{12} = 121.4 and C_{44} = 75.4 for Cu, and C_{11} = 246.0, C_{12} = 134 and C_{44} = 28.7 for Nb (Hirth and Lothe, 1982).

4.1. Traction continuity and periodic properties

Figs. 2a-f show the stress (or traction) fields (σ_{13} σ_{23} and σ_{33}) induced by the dislocation array (a–c) and the corresponding single dislocation (d–f). The single mixed dislocation is located at (X_0,Z_0)=(0, 5 nm) and the period length L is 10 nm for the mixed dislocation array case. All the stresses in Fig. 2 are normalized by the effective shear modulus of copper, ($C_{11}-C_{12}+C_{44}$) /3, defined in the plane {111} of the cubic crystal (Hirth and Lothe, 1982; Scattergood and Bacon, 1957; Chu et al. 2011b). It is clearly observed from these figures that the traction continuity at the interface z = 0 and the periodic properties of the stresses along the x- axis are satisfied. It is actually interesting to point out that, under either a single dislocation or a dislocation array and across the interface, while the contours of σ_{33} have a smooth tangent (c and f), the slope of the contours of σ_{13} σ_{23} are not (a,b,d,e).

As expected, singularity occurs at the core region, as shown in Fig. 2. Since this is dominated by the full-plane part in the strain expression in Eq. (15) when the field point approaches the source point (X_0,Z_0), the contribution from the image part can be neglected when the field point is close to the dislocation core region. However, away from the core, the stress field due to the dislocation array is adjusted and the periodic property along the x-direction is formed, whilst the magnitude of the stress field due to a single dislocation decreases gradually with increasing distance from the core. Furthermore, at most field points outside the core region, the magnitude of the traction due to a single dislocation is larger than that due to the corresponding dislocation array. This phenomenon is further analyzed below.

4.2. Influence of the dislocation array density on the traction

Since the interface is often the source for dislocation nucleation, the nucleation-driven stresses at the interface, especially the shear stresses, are important. Weak interfaces are expected to be sheared easily (Hoagland et al., 2002). Shown in Fig. 3a-c are the tractions at the interface due to the same mixed dislocation array with different densities (or period lengths). In the calculation, the distance between the dislocation array and the interface is fixed at 5 nm but the period length of the array varies. The variation of the tractions (σ_{13}, σ_{23} and σ_{33}) along the interface for different period lengths are shown in Fig. 3a, b and c, respectively. It is noticed that, as the period length approaches infinity, the results from the dislocation array are reduced to those from a single dislocation (obtained from the solutions to a single dislocation as independent check of the formulation for the dislocation array). From Fig. 3, it is further found that: (1) The maximum magnitude of these tractions all decrease with decreasing period length, which is consistent with the observation in Fig. 2. Namely, the stress fields (σ_{13}, σ_{23} and σ_{33}) are suppressed by the dislocation array. For instance, the absolute value of the maximum σ_{13} decreases from ~0.011 μ_e due to a single dislocation (or the period length $L=\infty$) to ~0.0063 μ_e due to the dislocation array with the period length L = 10 nm. (2) Individual traction components decrease with different decay rates as L decreases. The shear stress σ_{23} as shown in Fig. 3b has a largest decay rate, whilst the normal stress σ_{33}, as shown in Fig. 3c has the smallest, with the rate of the stress σ_{13} in Fig. 3a in between. (3) The location where the maximum magnitude of the traction occurs at the interface varies with the period length of the array, which implies that the possible interface-dislocation-nucleation site would also change. (4) The sites to reach the extreme value of the shear stresses σ_{13} and σ_{23} at the interface in case of a single dislocation are also different, as shown in Fig. 3a and 3b, which means that there are two possible sites to nucleate dislocations depending upon the relative contributions from both σ_{13} and σ_{23}. However, with decreasing period length, the two separated sites are gradually merged (i.e., for L = 10 nm). Thence only one set of nucleation points needs to be considered in the interface-dislocation-nucleation problem when the density of the dislocation array is relative high (or with relatively small period length). We should point out that these interesting features discussed above are associated with the traction components only; the variation of the in-plane stress components σ_{11}, σ_{22} and σ_{12} are totally different and the maximum values of these stress components could increase with increasing dislocation density. For instance, shown in Fig. 3d is the shear stress on the glide plane {111}; its maximum value increases slightly with increasing dislocation density.

4.3. Influence of dislocation array density on the P–K force

The image force or P–K force plays a critical role in the analysis of dislocation dynamics (Ghoniem and Han, 2005; Wang and Beyerlein, 2011; Zhou et al., 2010; Chu et al. 2012a, b). Generally, in order to move, a dislocation has to overcome the repulsive force induced by a hard interface, and the attractive force by a soft interface or free surface (Shehadeh et al., 2007). For the Cu/Nb binary system, Nb is often regarded as hard material since the effective shear modulus μ_e (Nb) = 46.9 GPa is larger than μ_e (Cu) = 40.8 GPa. Thence, the dislocation in the upper Cu half plane will be influenced by the relatively hard Cu/Nb interface. To check this conventional prediction, we first use the artificial binary system: Cu/αNb, in which the stiffness of αNb is equal to the stiffness of niobium times the coefficient α. The numerical results of P–K forces with respect to different α are shown in Fig. 4. In the calculation, the period length of the mixed dislocation array is fixed at L = 10 nm. It is observed from Fig. 4: (1) as is expected, overall, the magnitude of

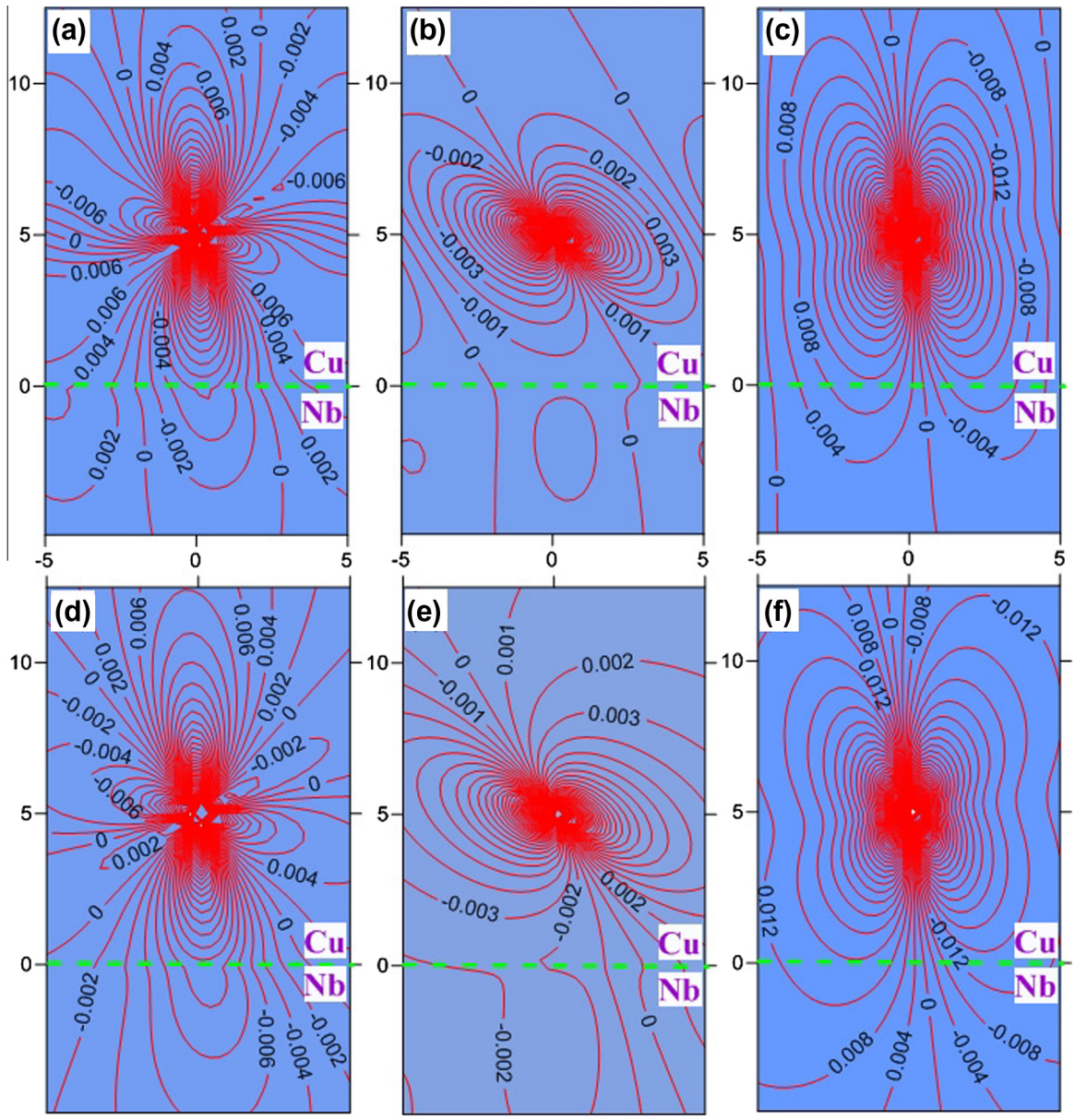

Fig. 2. Contours of stress fields due to a single mixed dislocation (½[101] on {111}) and the corresponding dislocation array (the horizontal axis is x, and vertical axis is z, and their units are both in nm): Shear stress σ_{13} in (a), shear stress σ_{23} in (b), and normal stress σ_{33} in (c), due to the dislocation array; shear stress σ_{13} in (d), shear stress in σ_{23} (e), and normal stress σ_{33} in (f), due to the single dislocation. The source point of the single mixed dislocation is at (0, 5 nm) and the dislocation array is 5 nm away from the interface with a period length L = 10 nm. The stresses are normalized by the effective shear modulus of copper defined by $\mu_e = (C_{11} - C_{12} + C_{44})/3$.

the P–K force decreases gradually with increasing distance of the array from the interface; (2) free surface ($\alpha = 0$) attracts the dislocation as predicted; (3) with increasing coefficient α (i.e. the stiffness of the lower half plane increases), the attractive force gradually decrease its algebraic value. Finally it changes its sign and becomes a repulsive force. This phenomenon is also consistent with the traditional prediction; (4) however, for the real Cu/Nb ($\alpha = 1$), the P–K force on the dislocation in copper is not repulsive force as commonly thought; it is actually attractive when the distance $d < 6.2$ nm and repulsive when $d > 6.2$ nm. This interesting feature is explained below: for the case of anisotropic material or bimaterial, the energy analyses due to a dislocation are more complicated. The P–K force depends on the crystal material and dislocation orientations relative to the global interface coordinates. For instance, graphite is quite easy to be sheared in the c-plane as compared to the other directions. Furthermore, the anisotropy ratio ($A = 2C_{44}/(C_{11} - C_{12})$) is 3.2 for Cu and 0.5 for Nb. They are quite deviated from the isotropic case ($A = 1.0$). Thus, in the Cu/Nb system studied here, the relative relationship between the two materials, hard or soft with respect to the dislocation move, depends on the anisotropy property, crystal orientation, and dislocation orientation. Thence, when one claims that one material is harder than the other, one needs to be extremely cautious.

It should be noted that Weertman (1965) proposed a different approach to evaluate the force acting on the dislocation, in which the stress in the P–K force in Eq. (18) was replaced by the deviatoric stress. The numerical results based on this modified method show that, although its magnitude is different, the trend of the P–K force is the same as in Fig. 4. This further confirms that our discussions and statements here are valid.

The influence of the period length of the mixed dislocation array on the P–K force in real Cu/Nb bimaterial is shown in Fig. 5. It is observed that: (1) Generally, the magnitude of the P–K force decreases with decreasing period length. (2) The influence of the

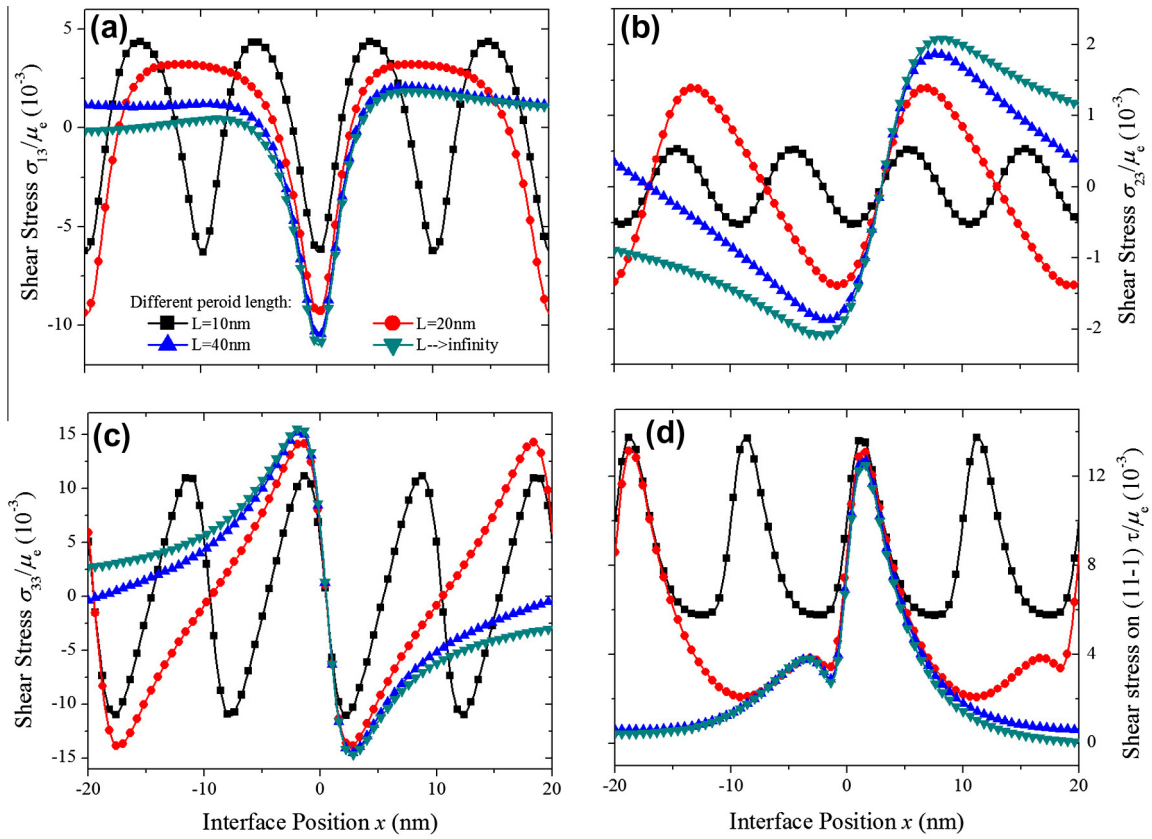

Fig. 3. Variation of the traction/stress on the interface/glide plane for different densities of the mixed dislocation array: Shear traction σ_{13} at the interface in (a), shear traction σ_{23} at the interface in (b), normal traction σ_{33} at the interface in (c), and shear stress τ on glide plane (11−1) in (d). The mixed dislocation array is 5 nm away from the interface and L is the period length between two adjacent dislocations in the dislocation array. When $L \to \infty$, the traction/stress due to the dislocation array is reduced to that due to a single dislocation.

dislocation array density on the P–K force decreases as the array approaches the interface. For instance, when the distance of the array to the interface is close to 2 nm, as shown in Fig. 5, different period length or dislocation density would have no effect on the P–K force. This is understandable since when the dislocation array is very close to the interface, the interaction between the dislocation array and interface and consequently the P–K force on the dislocation is dominated by the considered single dislocation itself only; the influence of other dislocations in the array can be neglected. (3) For fixed period length L = 10 nm, the P–K force changes its sign as the array approaches the interface. The critical

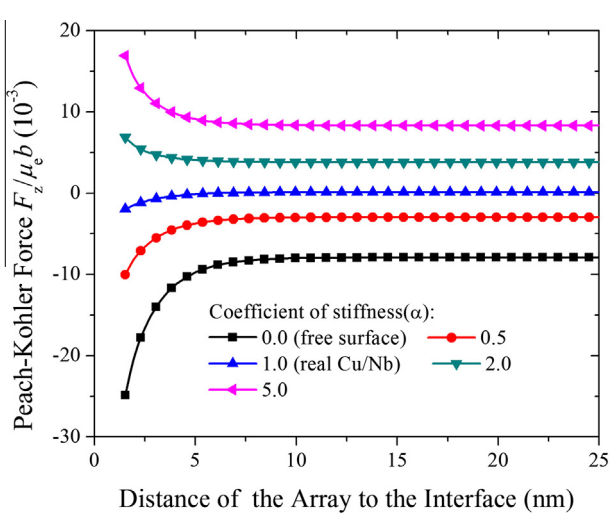

Fig. 4. Variation of the P–K force with the distance of dislocation array to the interface for different interface stiffness. The bimaterial model used here is an artificial binary material system Cu/αNb, in which the stiffness of material αNb is assigned by the stiffness of niobium times the coefficient α. The larger the coefficient α, the harder the interface is.

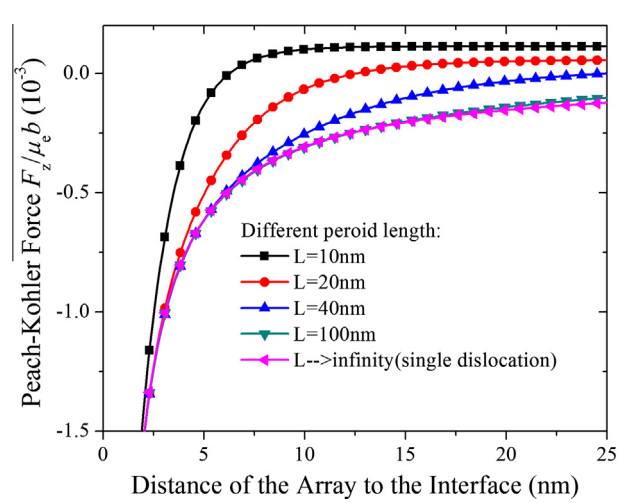

Fig. 5. Variation of the P–K force on the mixed dislocation (½[101]) with the distance of the dislocation array to the interface for different densities (or period length). The bimaterial model is Cu/Nb with the orientation of K–S {112} interface being described in the caption of Fig. 1.

distance between the array and the interface is at d≈6.2 nm. When the distance $d > 6.2$ nm, the P–K force is repulsive, and when $d < 6.2$ nm, it is attractive. To our best knowledge, this surprising phenomenon has not been reported in any previous literature. This interesting result further demonstrates that one should be very cautious when judging if the P–K force on a dislocation due to a bimaterial interface is attractive or repulsive.

In Figs. 4 and 5, only the z-direction P–K force is given. Actually, we have also calculated the P–K force in the x-direction. Numerical results show that the x-direction forces are zero under the tolerance of the numerical error. Physically, this result means that shifting the dislocation array along the x-direction with a small increment does not induce any change in the energy profile of the system. Thence, the x-direction force is zero. Since the other components of the P–K force are zero except that in z-direction, the glide force on the glide plane {111} can be obtained by projecting the P–K force F_z on the glide plane, which is equivalent to multiplying a constant coefficient (i.e., directional sine between the normal of the glide plane and z-direction). Thus the shape of the variation of the glide force is similar to the P–K force shown in Figs. 4 and 5.

In our numerical studies presented above, we focused on the mixed dislocation ½[101] on {111}. To investigate the influence of different Burgers vectors, we further consider the dislocation with Burger vector ½[-110] which is a screw type (along y-direction). The results are shown in Fig. 6. Different from the mixed dislocation discussed above, the P–K force is now repulsive. These interesting and different behaviors of the P–K forces on the screw and mixed dislocations can be explained via the following energy analysis: For a screw dislocation in a pure cubic crystal, Hirth and Lothe (1982) derived the energy coefficient K_s (See Eqs. (13–148) and (13–156) there) for the self-energy. For copper, $K_s = 42.1$ GPa while for niobium, $K_s = 44.3$ GPa, implying that the P–K force acting on a screw dislocation in Cu should be repulsive. On the other hand, for an edge dislocation (See Eqs. (13–149) and (13–156)), the energy coefficient $K_{ex} = 71.9$ GPa ($K_{ez} = 82.2$ GPa) for copper, $K_e = 60.0$ GPa for nobium, implying that the P–K force acting on edge dislocation in Cu should be attractive. The mixed dislocation ½[101] can be decomposed into a screw part and an edge part. The ratio of the magnitude of the edge part to screw part is $\sqrt{3} : 1$. Thus, the edge part will dominate the interaction and the P–K force on the mixed dislocation is attractive. Thus our numerical result is consistent with the theoretical energy analysis based on Hirth and Lothe (1982).

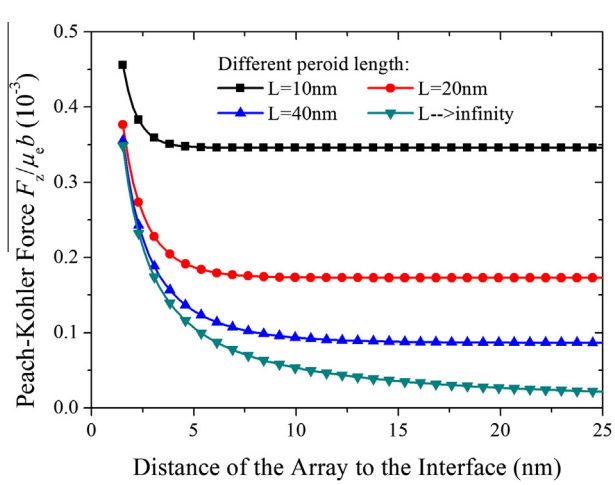

Fig. 6. Variation of the P–K force on the screw dislocation (½[−110]) with the distance of the dislocation array to the interface for different densities (or period lengths). The bimaterial model is Cu/Nb with the orientation of K–S {112} interface being described in the caption of Fig. 1.

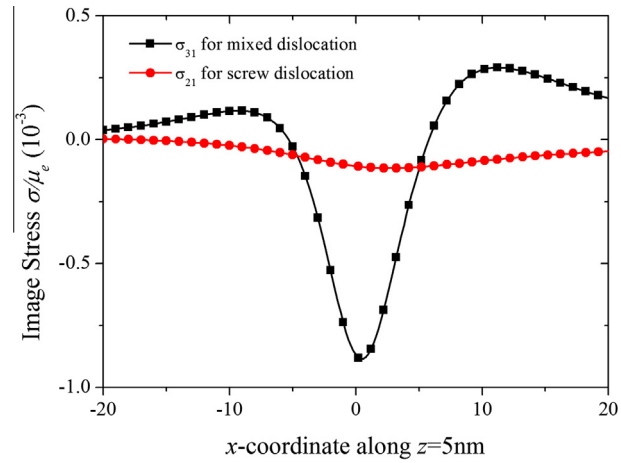

Fig. 7. Distribution of the image stress along x-axis (for fixed z = 5 nm) due to a single screw/mixed dislocation located at ($x = 0, z = 5$ nm). The mixed dislocation has a Burgers vector ½[101] and the screw dislocation has one as ½[−110]. The bimaterial model is Cu/Nb with the orientation of K–S {112} interface being described in the caption of Fig. 1.

Comparing Fig. 5 and Fig. 6, one may observe that the P–K force magnitude decreases with increasing dislocation density for the mixed dislocation while it increases with increasing dislocation density for the screw dislocation. This is the other interesting feature from our analysis, which can be further explained by the principle of superposition. According to Eq. (18), the P–K force is $F_z = b_2\sigma_{21}$ for the screw dislocation array and is $F_z = b_1\sigma_{11} + b_2\sigma_{21} + b_3\sigma_{31}$ for the mixed dislocation array. Furthermore, as discussed in Section 3, only the image stress has contributions to the P–K force. For the mixed dislocation ½[101] in the Cu/Nb K-S bimaterial, the magnitude of b_3 ($\approx 0.82b$) is larger than both b_1 ($\approx -0.29b$) and b_2 ($\approx -0.5b$) whilst the image stresses σ_{11} and σ_{21} are much smaller than σ_{31} (which can be seen from our exact closed-form solutions for the single dislocation case). Therefore, for the mixed dislocation case, one needs only to focus on the term $b_3\sigma_{31}$ in the P–K force expression. Consequently, the P–K behavior will be dominated by the image stress σ_{21} for the screw dislocation case and by σ_{31} for the mixed dislocation case. Keeping in mind that the image stresses due to the corresponding arrays can be obtained by superposing the image stresses induced by individual dislocations in the array we only need to analyze these image stresses due to a single dislocation. Fig. 7 shows the distribution of the image stresses along x-direction (for fixed z = 5 nm) induced by a dislocation located at ($x = 0, z = 5$ nm), σ_{21} by the screw dislocation and σ_{31} by the mixed dislocation. It is observed from Fig. 7 that for the mixed dislocation case, the sign of the image stress σ_{31} at $|x|>10$ nm is opposite to that at $x = 0$. Consequently, the magnitude of the total image stress due to the corresponding dislocation array will decrease. Therefore, the P–K force of the mixed dislocation array decreases with increasing dislocation density (or decreasing period length). On the other hand, as shown in Fig. 7, the sign of image stress σ_{21} due to a screw dislocation is the same in the calculated domain ($x = -20$ nm ~ 20 nm). Thus, the P–K force of the screw dislocation array increases with increasing dislocation density.

5. Conclusions

The strain/stress fields due to a dislocation array in an anisotropic bimaterial are studied in this paper. Main results and conclusions are summarized as follows:

(1) An analytical and simple expression is obtained by using the Cottrell summation formula, which avoids the item-by-item summation and thus greatly improve the accuracy and computation efficiency.
(2) It is found that the P–K force associated with the full-plane part of the stress field due to a dislocation array is exactly zero, which greatly simplifies the computation of the P–K force. This property is verified both mathematically and physically.
(3) Numerical results for the Cu/Nb bimaterial with the K-S interface demonstrate that the traction continuity on the interface and the period condition along the dislocation array are exactly satisfied under the tolerance of computation error.
(4) By comparing the stress fields at the Cu/Nb K-S interface due to a single dislocation to those due to a dislocation array, it is found that the tractions on the interface are suppressed with increasing dislocation density (not for all the field points, but for most of them), whist the shear component on the glide plane {111} increases slightly with increasing dislocation density.
(5) It is found that the Cu/Nb K-S interface attracts the mixed dislocation array with Burgers vector ½[101] in copper, whilst it repels the screw dislocation array with Burgers vector ½[−110]. This interesting result implies that the P–K force depends not only on the material property, but also on the crystal orientation and the Burgers vector orientation relative to the global coordinates of the bimaterial.

Acknowledgments

Chu acknowledgments the support provided by Shanghai Eastern-Scholar Plan and by State Key Laboratory for Mechanical Behavior of Materials. The authors are very grateful to Prof. J. P. Hirth in Washington State University and Dr. J. Wang in Los Alamos National Laboratory for their helpful discussions. Constructive suggestions from the reviewers and Editor-in-Chief Prof. David Hills are also acknowledged.

References

Barnett, D.M., Lothe, J., 1974. An image force theorem for dislocations in anisotropic bicrystals. J. Phys. F: Met. Phys. 4, 1618–1635.
Beausir, B., Fressengea, C., 2013. Disclination densities from EBSD orientation mapping. Int. J. Solids Struct. 50, 137–146.
Cai, W., Bulatov, V.V., Chang, J.P., Li, J., Yip, S., 2001. Anisotropic elastic interactions of a periodic dislocation array. Phys. Rev. Lett. 86, 5727–5730.
Chen, K.X., Dai, Q., Lee, W., Kim, J.K., Schubert, E.F., Grandusky, J., Mendrick, M., Li, X., Smart, J.A., 2008. Effect of dislocations on electrical and optical properties of *n*-type $Al_{0.34}Ga_{0.66}N$. Appl. Phys. Lett. 93, 192108.
Chou, Y.T., 1962. Interaction of parallel dislocations in a hexagonal crystal. J. Appl. Phys. 33, 2747–2751.
Chou, Y.T., Lin, L.S., 1975. Instability of edge dislocation walls in a two-phase isotropic medium. Mater. Sci. Eng. 20, 19–27.
Chu, H.J., Pan, E., Wang, J., Beyerlein, I.J., 2011a. Three-dimensional elastic displacements induced by a dislocation of polygonal shape in anisotropic elastic crystals. Int. J. Solids Struct. 48, 1164–1170.
Chu, H.J., Wang, J., Zhou, C.Z., Beyerlein, I.J., 2011b. Self-energy of elliptical dislocation loops in anisotropic crystals and its application for defect-free core/shell nanowires. Acta Mater. 59, 7114–7124.
Chu, H.J., Pan, E., Han, X., Wang, J., Beyerlein, I.J., 2012a. Elastic fields of dislocation loops in three-dimensional anisotropic bimaterials. J. Mech. Phys. Solids 60, 418–431.
Chu, H.J., Pan, E., Wang, J., Beyerlein, I.J., 2012b. Elastic displacement and stress fields induced by a dislocation of polygonal shape in an anisotropic elastic half-space. J. Appl. Mech. 79, 021011.
Cottrell, A.H., 1953. Dislocation and Plastic Flow in Crystals. Oxford University Press, Fair Lawn (New Jersey).
de Geus, T.W.J., Peerlings, R.H.J., Hirschberger, C.B., 2014. An analysis of the pile-up of infinite periodic walls of edge dislocations. Mech. Res. Commun. 54, 7–13.
Dundurs, J., Mura, T., 1964. Interaction between an edge dislocation and a circular inclusion. J. Mech. Phys. Solids 12, 177–189.
Eshelby, J.D., 1951. The force on an elastic singularity. Phil. Trans. R Soc. Lond. A–Math. Phys. Sci. 244, 87–112.
Ghoniem, N.M., Han, X., 2005. Dislocation motion in anisotropic multilayer materials. Philos. Mag. 85, 2809–2830.
Gosling, T.J., Willis, J.R., 1994a. A line-integral representation for the stresses due to an arbitrary dislocation in an isotropic half-space. J. Mech. Phys. Solids 42, 1199–1221.
Gosling, T.J., Willis, J.R., 1994b. The energy of arrays of dislocation in an anisotropic half-space. Philos. Mag. A 69, 65–90.
Gutkin, M.Y., Enzevaee, C., Shodja, H.M., 2013. Interface effects on elastic behavior of an edge dislocation in a core–shell nanowire embedded to an infinite matrix. Int. J. Solids Struct. 50, 1177–1186.
Hartley, C.S., 1969. The stress fields of uniformly spaced, infinite edge dislocation arrays in a semi-infinite isotropic solids. Scr. Metall. 3, 607–612.
Hirth, J.P., Barnett, D.M., Lothe, J., 1979. Stress fields of dislocation arrays at interfaces in bicrystals. Philos. Mag. A 40, 39–47.
Hirth, J.P., Lothe, J., 1982. Theory of Dislocations, second ed. Wiley, New York.
Hoagland, R.G., Mitchell, T.E., Hirth, J.P., Kung, H., 2002. On the strengthening effects of interfaces in multilayer fee metallic composites. Philos. Mag. A 82, 643–664.
Kang, K., Wang, J., Zheng, S.J., Beyerlein, I.J., 2012. Minimum energy structures of faceted incoherent interfaces. J. Appl. Phys. 112, 073501.
Krasavin, S., 2009. Electron scattering due to dislocation wall strain field in GaN layers. J. Appl. Phys. 105, 126104.
Liu, L., Wang, J., Gong, S.K., Mao, S.X., 2011. High resolution transmission electron microscope observation of zero-strain deformation twinning mechanisms in Ag. Phys. Rev. Lett. 106, 175504.
Lubarda, V.A., Kouris, D.A., 1996. Stress fields due to dislocation arrays at interfaces. Mech. Mater. 23, 191–203.
Lubarda, V.A., 1997. Energy analysis of dislocation arrays near bimaterial interfaces. Int. J. Solids Struct. 34, 1053–1073.
Misra, A., Verdier, M., Lu, Y.C., Kung, H., Mitchell, T.E., 1998. Structure and mechanical properties of Cu-X (X = Nb, Cr, Ni) nanolayered composites. Scr. Mater. 39, 555–560.
Mura, T., 1963. Continuous distribution of moving dislocations. Philos. Mag. 8, 843–857.
Mura, T., 1987. Micromechanics of Defects in Solids. Martinus Nijhoff, Dordrecht.
Nakahara, S., Wu, J.B.C., Li, J.C.W., 1972. Dislocations in a welded interface between two isotropic media. Mater. Sci. Eng. 10, 291–296.
Ohno, Y., Tokumoto, Y., Yonenaga, I., Fujii, K., Yao, T., 2012. Optical properties of edge dislocations on (1–100) prismatic planes in wurtzite ZnO introduced at elevated temperatures. J. Appl. Phys. 111, 113514.
Otsuka, K., Kuwabara, A., Nakamura, A., Yamamoto, T., Matsunaga, K., Ikuhara, Y., 2003. Dislocation-enhanced ionic conductivity of yttria-stabilized zirconia. Appl. Phys. Lett. 82, 877–879.
Pan, E., Yuan, F.G., 2000. Three-dimensional Green's functions in anisotropic bimaterials. Int. J. Solids Struct. 37, 5329–5351.
Pan, E., 2003a. Three-dimensional Green's functions in an anisotropic half-space with general boundary conditions. J. Appl. Mech. 70, 101–110.
Pan, E., 2003b. Some new three-dimensional Green's functions in anisotropic piezoelectric bimaterials. Electron. J. Boundary Elem. 1, 236–269.
Pennycook, S.J., 2008. Investigating the optical properties of dislocations by scanning transmission electron microscopy. Scanning 30, 287–298.
Rey, C., Saada, G., 1975. The elastic field of periodic dislocation networks. Philos. Mag. 33, 825–841.
Scattergood, R.O., Bacon, D.J., 1957. The Orowans mechanism in anisotropic crystals. Philos. Mag. 31, 179–198.
Shehadeh, M.A., Lu, G., Banerjeez, S., Kioussis, N., Ghoniem, N., 2007. Dislocation transmission across the Cu/Ni interface: a hybrid atomistic–continuum study. Philos. Mag. 87, 1513–1529.
Stroh, A.N., 1958. Dislocations and cracks in anisotropic elasticity. Philos. Mag. 3, 625–646.
Stroh, A.N., 1962. Steady state problems in anisotropic elasticity. J. Math. Phys. 41, 77–102.
Subramaniyan, A.K., Sun, C.T., 2008. Continuum interpretation of virial stress in molecular simulations. Int. J. Solids Struct. 45, 4340–4346.
Tan, E.H., Sun, L.Z., 2006. Stress field due to a dislocation loop in a heterogeneous thin film-substrate system. Model. Simul. Mater. Sci. Eng. 14, 993–1013.
Tan, E.H., Sun, L.Z., 2011. Dislocation-induced stress field in multilayered heterogeneous thin film system. J. Nanomech. Micromech. 1, 91–103.
Ting, T.C.T., 1996. Anisotropic Elasticity. Oxford University Press, Oxford.
Wang, Z.Q., Beyerlein, I.J., 2011. An atomistically-informed dislocation dynamics model for the plastic anisotropy and tension–compression asymmetry of bcc metals. Int. J. Plast. 27, 1471–1484.
Weertman, J., 1965. The Peach-koehler equation for the force on a dislocation modified for hydrostatic pressure. Phil. Mag. 11, 1217–1223.
Zhou, C.Z., Biner, S.B., LeSar, R., 2010. Discrete dislocation dynamics simulations of plasticity at small scales. Acta Mater. 58, 1565–1577.
Zhu, T., Li, J., 2010. Ultra-strengthen materials. Prog. Mater. Sci. 55, 710–757.